Estimation of power input and output of structures using structural intensity measurements

Peter Groba[1], Johannes Ebert[1], Torsten Stoewer[1], Joachim Bös[2], Tobias Melz[2]
[1] BMW Group, Structural Dynamics and Analysis, 80788 Munich, Germany , Email: peter.groba@bmw.de
[2] TU Darmstadt, System Reliability, Adaptive Structures, and Machine Acoustics SAM, 64289 Darmstadt, Germany

Introduction

The numerical analysis of a vehicle body's acoustical behavior gets increasingly more important in the product design process. A way to describe structure-borne sound phenomena is to gather information on the energy flow through the usage of the structural intensity (STI). The STI creates a link between the excitation of a structure and its sound radiation. A further calculation of power values based on the STI allows for the description of the power input and output into certain areas of a structure. Thus, the identification of energy sinks and sources is possible.

Numerous studies in this context are related to the measurement of energetic quantities and the comparison of measurement results with analytical or numerical calculations. This work introduces the calculation basis to obtain power values from measurement data. It uses two approaches to compute power quantities from the STI. The first step is the calculation and assessment of the input power for a rectangular plate with an external energy source. Then, a more complex structure is analyzed. This analysis aims at the acquisition of information on the energy input and output of indirectly excited structural components by means of power balance calculations.

Energy balance equations

Analogous to the sound intensity in fluids, the STI depicts the energy flow within solid structures. In the frequency domain it results from the cross-spectral density of the complex stresses $\underline{\mathbf{S}}$ and the related conjugated complex velocities $\underline{\mathbf{v}}^*$ [1, 2]:

$$\underline{\mathbf{I}}_\mathrm{s}(f) = -\frac{1}{2}\underline{\mathbf{S}}(f) \cdot \underline{\mathbf{v}}^*(f). \tag{1}$$

This study assesses thin-walled structures for which the Kirchhoff theory applies. In this case the three dimensional problem from Equation (1) is reduced to a two dimensional problem, as the energy flow normal to the plane is negligible. The multiplication of the complex section forces $\underline{N}, \underline{Q}$ and moments $\underline{M}$ with the velocities $\underline{v}$ and $\underline{\dot{\varphi}}$, respectively, yields the STI for plates

$$\underline{\mathbf{I}}'(f) = -\frac{1}{2}\begin{bmatrix} \underline{N}_x\underline{v}_x^* + \underline{N}_{xy}\underline{v}_y^* + \underline{M}_x\underline{\dot{\varphi}}_y^* - \underline{M}_{xy}\underline{\dot{\varphi}}_x^* + \underline{Q}_x\underline{v}_z^* \\ \underline{N}_y\underline{v}_y^* + \underline{N}_{yx}\underline{v}_x^* - \underline{M}_y\underline{\dot{\varphi}}_x^* + \underline{M}_{yx}\underline{\dot{\varphi}}_y^* + \underline{Q}_y\underline{v}_z^* \end{bmatrix}. \tag{2}$$

The prime $'$ denotes that $\underline{\mathbf{I}}'(f)$ is integrated over the thickness h of the plate. Thus, it yields the complete energy flowing through a cross section of the structure.

Analyses with regard to the energetic behavior of structures mainly focus on the active energy flow $\mathbf{I}_{\mathrm{s,a}}(f)$. In the frequency domain it corresponds to the real part of the complex STI, which in turn is equivalent to the time-averaged value of the energy flow $\langle \mathbf{I}_\mathrm{s}(t) \rangle$ in the time domain:

$$\mathbf{I}_{\mathrm{s,a}}(f) = \mathrm{Re}\left(\underline{\mathbf{I}}_\mathrm{s}(f)\right) = \langle \mathbf{I}_\mathrm{s}(t) \rangle. \tag{3}$$

Figure 1 depicts the absolute value of a car floor panel's energy flow and gives an example of the energy distribution in a structure. In order to obtain complete information about the energy flow, its direction needs to be described likewise. However, combining data about the energy density distribution and the energy flow direction delivers complex information, and thus hampering the usage of the STI as an indicator for the application of design modifications.

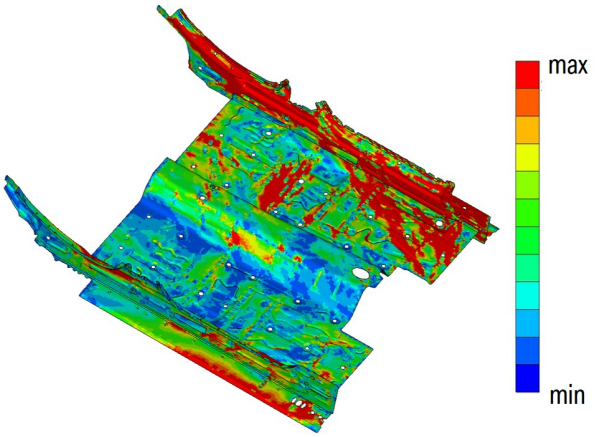

Figure 1: Energy distribution in a car floor panel.

As an intermediate step, the information gained via intensity calculations (vector quantity) is transformed to scalar values. This preparatory simplification is supposed to support the derivation of reliable design rules based on a structure's energetic behavior in future studies. Here, the estimation of power values as the chosen approach rests on the first law of thermodynamics. It states that in a defined system energy is neither created nor destroyed but conserved at all time [3]. Consequently, a simplified balancing equation for steady-state vibrations in the frequency domain

$$\iint_{A_\mathrm{s}} \mathbf{I}_\mathrm{s}(f)\mathbf{n}_\mathrm{s}\mathrm{d}A = P_{\mathrm{s,in}}(f) - P_{\mathrm{s,diss}}(f) \tag{4}$$

is derived. Equation (4) links the surface integral of the STI to the difference between the input power $P_{\mathrm{s,in}}$ and the dissipated power $P_{\mathrm{s,diss}}$ in defined closed boundaries. The STI calculated via Equation (2) is already integrated over the thickness of the structure. Thus, using $\underline{\mathbf{I}}'(f)$ in the calculation, the power balance can be computed via line integration over a closed boundary $\mathrm{d}l$

$$P_{\mathrm{STI}}(f) = \int_{l_{\mathrm{s}}} \mathbf{I}'(f)\mathbf{n}_{\mathrm{s}}\mathrm{d}l. \tag{5}$$

Furthermore, another calculation approach is introduced. Its results are compared to those obtained from Equation (5). The second approach is based on the integration of the STI's divergence over the surface of the structure $\mathrm{d}A$

$$P_{\mathrm{div}}(f) = \iint_{A_{\mathrm{s}}} \mathrm{div}(\mathbf{I}'(f))\mathrm{d}A. \tag{6}$$

Structural intensity measurements

Equation (2) is not feasible for experimental analyses, because the section forces and moments are difficult to access. In contrast, displacements, velocities, or accelerations are quantities that can be rather easily determined in measurements. An equation using these quantities is given in [1]:

$$\begin{aligned} I'_x = -\frac{B}{2h}\Bigg(&\left(\frac{\delta^2 w}{\delta x^2} + \nu\frac{\delta^2 w}{\delta y^2}\right)\left(\frac{\delta \dot{w}}{\delta x}\right)^* \\ &+(1-\nu)\frac{\delta^2 w}{\delta x \delta y}\left(\frac{\delta \dot{w}}{\delta y}\right)^* \\ &-\frac{\delta}{\delta x}\left(\frac{\delta^2 w}{\delta x^2} + \frac{\delta^2 w}{\delta y^2}\right)(\dot{w})^*\Bigg). \end{aligned} \tag{7}$$

Equation (7) represents an approximation for the x-component of the STI as a function of the displacements w and velocities $\dot{w}$ normal to the plane. The y-component is derived equally by interchanging x and y. The derivation of such an approximate solution is done so by neglecting the in-plane components of the STI, which are represented by the normal forces $\underline{N}$ in Equation (2). The next step in the estimation of the STI from measurement data is to find feasible ways to solve Equation (7). There are two different approaches used, where both approaches make it necessary to gather data in the vicinity of a reference point (i, j), see Figure 2.

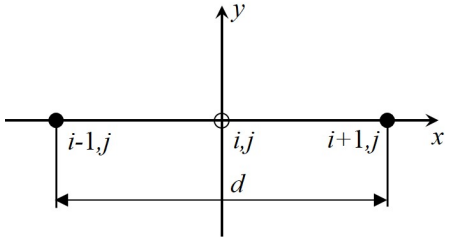

Figure 2: Position of measurement points in the vicinity of a reference point (i, j).

The first approach is the so-called two-transducer method, which was introduced by Noiseux [4]

$$\begin{aligned} I'(x) = \frac{\sqrt{Bm'}}{hd\omega^2}\Big[&2\,\mathrm{Im}\left\{\underline{a}_{i-1,j}(\omega)\underline{a}^*_{i+1,j}(\omega)\right\} \\ &+\mathrm{i}\left(\left|\underline{a}_{i-1,j}(\omega)\right|^2 - \left|\underline{a}_{i+1,j}(\omega)\right|^2\right)\Big] \end{aligned} \tag{8}$$

and uses complex accelerations $\underline{a}$ in the intensity's calculation. The necessary data is gathered at the measurement points $(i-1, j)$ and $(i+1, j)$, which possess the distance d towards each other. The second approach is the gradient method. It uses numerical differentiation to solve the spatial derivations in Equation (7) [2]. Here, the central differential quotient

$$\frac{\delta w}{\delta x} = -\frac{w(i+1,j) - w(i-1,j)}{2\Delta x} + \mathrm{O}(\Delta x^2) \tag{9}$$

is used, where $2\Delta x$ equals d.

Estimate the power input in a simple test structure

For the first attempt to estimate power values a simple test setup was selected. A rectangular aluminum plate is clamped between two frames and thin wire. This is done in order to represent "simply supported" boundary conditions, only blocking the translational degree of freedom in the direction normal to the plate. The necessary measurements are conducted with a laser scanning vibrometer. Figure 3 shows the structure with the mesh grid. The distance between the measurement points is 20 mm.

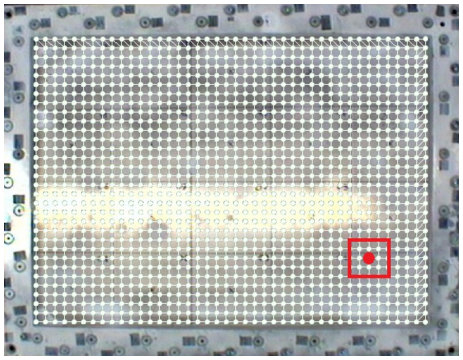

Figure 3: Setup of the test structure – mesh grid and area of excitation (red markings).

The measurements are conducted in a frequency range up to 1000 Hz. The structure's natural frequencies are determined via modal analysis. The evaluation of data is conducted for the excitation of the structure in these frequencies. The respective modes are henceforth called excitation modes. For a better distinction between each value, the results are labeled according to the order of the natural frequencies' occurrence.

In this study, the integration limits in Equation (5) and (6) are determined by setting a rectangular balancing area with a distance of 40 mm between each edge and the excitation point (red square in Figure 3). The results

for P_{STI} and P_{div} are shown in Figure 4 and 5, respectively. Each graph contains the results for the aforementioned approximation methods: two-transducer method, '2-trans.', and gradient method, 'grad.'.

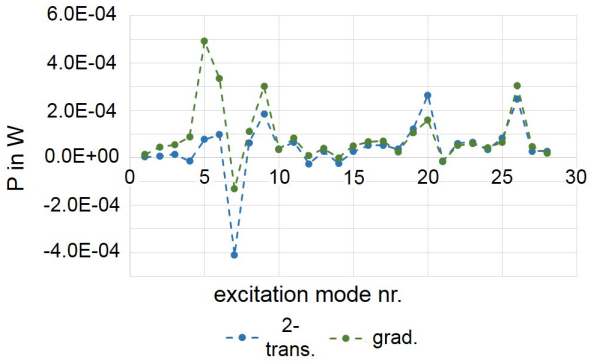

Figure 4: Estimated curve progression of P_{STI}.

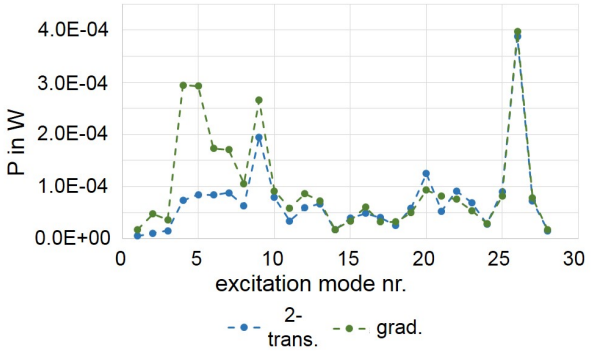

Figure 5: Estimated curve progression of P_{div}.

Commencing at the ninth excitation mode ($\approx 321\,\mathrm{Hz}$) the power quantities, P_{STI} and P_{div}, show a good accordance regarding their curve progression and value range for calculations based on the STI estimated via two-transducer method and gradient method, respectively. The scattering of the measurement data for lower frequencies leads to deviations in the results of the calculated STI [2]. It is plausible that in case of faulty source data the outcome of the power calculation is likewise incorrect. A comparison between P_{STI} and P_{div} with a reference solution has shown that results gathered via the gradient method exhibit a better accordance with the curve progression of the reference solution, commencing already at the fourth excitation mode ($\approx 154\,\mathrm{Hz}$). This matches the limitations poised by the two-transducer method, which is not valid at near-field conditions, and therefore exhibits a frequency dependent minimum distance to discontinuities. The graphs for P_{STI} in Figure 4 contain negative values for certain frequencies, however, this is not plausible. The calculations are conducted close to the excitation point and all power values should be positive, as is the case for P_{div}. It is assumed that this behavior is due to a higher sensitivity of the STI integration to errors in the direction of the energy vectors.

The estimated power values show consistent results for both approximation methods of the STI and both power calculation approaches, respectively. However, the correspondence with a reference signal is not satisfactory. This will be the topic of future studies including further error evaluation of the introduced power results.

Analysis of a complex structure

The analysis in the previous section shows that the derived power values are able to depict the quality of the power input with several restrictions. The next step is the analysis of a more complex setup (see Figure 6). It consists of two aluminum plates, connected by four aluminum cylinders. The lower plate is simply supported and excited by an external force. The upper plate exhibits no external energy input. Therefore, the necessary energy to induce vibrations in the upper plate needs to be transferred via the connecting cylinders.

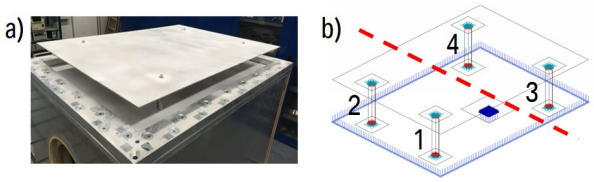

Figure 6: Setup of complex test structure: a) real setup and b) graphical representation of boundary conditions.

Figure 7 shows the results of the STI for the 28th excitation mode. It exhibits a high similarity regarding energy direction and distribution in measurement and numerical simulations. Both results show a widely spread vortex with a high energy density in the right part of the structure. Furthermore, the distribution of vortices and energy direction exhibit similarities over a great share of the analyzed structure. An important difference exists regarding the energy density at the connections between plate and cylinders. In case of the simulation's results the energy density in these areas is enhanced, see red marks in Figure 7 b). This elevation is not present in the measurement data.

In a first analysis, P_{STI} and P_{div} are calculated for the cylinders' positions. The integration limits are the same as in the previous section. For this case the evaluation of the calculated results yields no consistent outcome when comparing P_{STI} and P_{div} against one another. In addition, the summation of the power values from the four cylinder positions yields a large number of negative results. This is not plausible since the cylinders are the energy sources for the upper plate, where the sum of all values should be positive. This is the result that can be found when evaluating respective numerical simulations.

The evaluation of the data at the cylinders' positions yields no satisfactory results, thus the analysis is simplified. As depicted in Figure 6 b), the upper plate of the structure is split in two parts. In this way the boundary, at which the estimation of power values is conducted, moves further away from the discontinuities present in the structure. Figure 8 shows results for measurement and numerical simulation for two different ex-

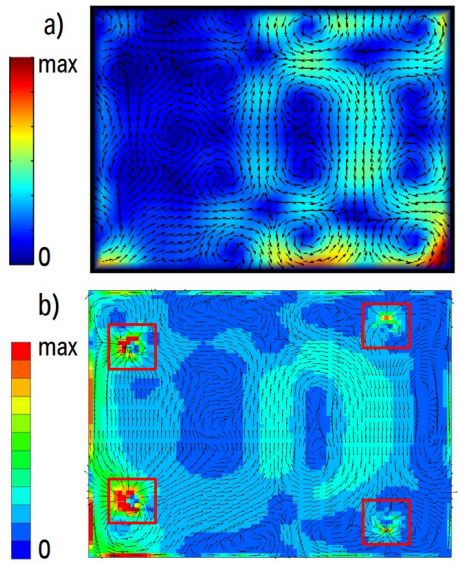

Figure 7: Depiction of energy distribution (color scale) and energy direction (arrows) from a) measurement and b) numerical simulation for the 28th excitation mode of the structure.

citation modes. The white arrows indicate some of the main energy paths for each result. For the 28th mode, the results are consistent for both measurement and numerical solution, whereas the energy flow is reversed in the results for the 46th mode.

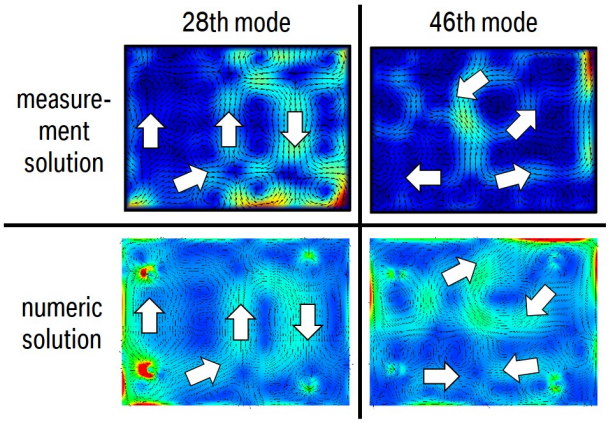

Figure 8: Results for measurement data and numerical simulation of the upper plate for the 28th and 46th excitation mode.

The analysis of the energy flow distribution alone is not sufficient to allow for a reliable statement concerning the general direction of the energy propagation. The calculation of power values is done by referring to the right part of the upper plate. Table 1 gives an overview of the algebraic signs of the results. A positive value of the power balance indicates that the energy input through the cylinders is higher than the output and the energy dissipation, thus there is a net energy flow from this region to the rest of the plate as it was the case for the excitation area of the rectangular plate. On the contrary, a negative value shows that the energy is flowing into the balanced right side of the structure and further propagates to the lower plate. In case of the 28th excitation mode all power values show an accordance in their algebraic sign and are indicating an energy flow from the left to the right side of the structure. For the 46th excitation mode the reversed energy flow between numerical and measurement result leads to opposite signs of the results. Thus, the power values indicate a reversed energy flow between both results.

Table 1: Algebraic signs of power balance value results.

excitation mode	numerical solution	experimental solution	
		2-trans.	grad.
28	negative	negative	negative
48	positive	negative	negative

On the basis of a reversed energy flow it seems plausible that the outcome of the power calculation is equally reversed. Nevertheless, the results from measurement and numerical simulation show differences that make further analysis necessary.

Conclusion

Two different approximation methods are used to calculate the STI from measurement results. They are the foundation for the calculation of P_{STI} and P_{div}, which are used to estimate the power input in a rectangular plate. For higher frequencies, both approximation methods show a good accordance for both power values. The analysis of more complex structures needs to be continued, as it could be shown exemplarily that the power values deliver plausible results based on the underlying energy flow. The findings indicate that energy flow measurements and connected power calculations can be used to describe the energy propagation. However, future studies need to further assess the accuracy of the approach and a deeper analysis of the introduced complex structure seems necessary in order to verify the observed results.

Acknowledgement

The author would like to thank Mr. Florian Assenbrunner, who contributed to this work with the necessary measurements and preliminary analyses.

References

[1] Meudt, P.: Strukturintensitätsanalyse in der Maschinenakustik. Dissertation, Technische Universität Darmstadt, 1998

[2] Buckert, S.: Bewertung adaptiver Strukturen auf Basis der Strukturintensität. Dissertation, Technische Universität Darmstadt, 2013

[3] Theodore, L., Ricci, F. and van Vliet, T.: Thermodynamics for the practicing engineer. Wiley, Hoboken, 2009

[4] Noiseux, D.U.: Measurement of power flow in uniform beams and plates. Journal of the Acoustical Society of America, 48(2), 1970, 238–247